Site Disorder in Ice VII Arising from Hydrogen Bond Fluctuations†

Chris Knight and Sherwin J. Singer*

Department of Chemistry, Ohio State University, Columbus, Ohio 43210

Received: March 30, 2009; Revised Manuscript Received: May 26, 2009

Recently, multisite models used for the refinement of neutron diffraction data have suggested that the structure of ice VII is quite unlike that of its ordered counterpart, ice VIII. We investigate the oxygen site disorder by modeling the site displacement, obtained from periodic DFT calculations, as a function of the local hydrogen bond network. Then, using graph invariants to describe hydrogen bond fluctuations in the thermodynamic limit, we perform statistical mechanical calculations using the oxygen site displacement model developed here. We find that the probability distribution of the oxygen atom about its perfect lattice site more closely resembles the ⟨100⟩ model rather than the recently suggested ⟨111⟩ model, although both models represent a simplification of the actual site distribution. We also find a unimodel distribution for the hydrogen bonded oxygen−oxygen distance and a trimodel distribution for the nearest nonbonded oxygen−oxygen distance with a peak separation of ∼0.1 Å.

1. Introduction

The proton-ordering phase transition of ice VII to antiferroelectric proton-ordered ice VIII is, in many respects, considered to be well-characterized. What is not well understood, however, is the apparent site disorder of the oxygen atoms suggested by recent neutron diffraction studies.[1−3] Studying ice VII in its region of stability, Kuhs et al. achieved a good fit to neutron diffraction data by treating the thermal motion of the oxygens anharmonically.[1] This model led to a surprisingly short O−D distance of 0.89 Å, which lengthened by 0.13 Å when this distance was allowed to vary freely after another refinement with a rigid water geometry. From this analysis, it appeared that there was significant motion along the set of ⟨100⟩ axes, suggesting disorder of the oxygen atoms about their perfect lattice sites. Here the symbol ⟨100⟩ stands for all axes related by symmetry to the [100] axis, for example: [100], [$\bar{1}$00], [010], [0$\bar{1}$0], [001], and [00$\bar{1}$]. Jorgensen and Worlton investigated the structure of ice VII using a time-of-flight neutron diffraction technique.[2] They also found it difficult to separate the static and thermal displacements of the oxygen atoms. Introducing a multisite model for the hydrogens did elongate the O−D distance somewhat, but it suggested angles that did not seem probable. Therefore, they also concluded that some displacement of the oxygen along the ⟨100⟩ directions, away from the covalently bonded deuteriums, would allow for the lengthening of the O−D distance.

More recently, an investigation by Nelmes et al. refined neutron diffraction data using various combinations of multisite models for both the oxygen and hydrogens treating the thermal motion harmonically.[3] A good fit of their models was measured by the closeness of the water molecule geometry to that found in ice VIII, the proton-ordered phase, with an O−D distance and D−O−D angle of 0.970 Å and 107.3°, respectively.[3] They found that the best fit was achieved when oxygen atoms were displaced along the set of ⟨111⟩ axes and the hydrogens shifted along three-fold sites surrounding the ⟨111⟩ axes. This gave an O−D distance and D−O−D angle of 0.977 Å and 107.1°, respectively. The best fit that could be achieved using the ⟨100⟩ axes for oxygen, with three-fold sites for hydrogens, resulted in a water geometry of 1.01 Å and 107°, which is consistent with the earlier work of Kuhs et al.[1] Regardless of model, all fits yielded site displacement magnitudes of 0.135 Å. The ⟨100⟩ model for oxygen displacement yielded H-bonded oxygen−oxygen distances of 2.833 and 2.839 Å, both in close agreement with their data from ice VIII under similar conditions. However, the ⟨111⟩ model, which gave the best water geometry overall, also predicted two sets of H-bonded oxygen−oxygen distances that were ∼0.1 Å longer and shorter than the H-bond distances in ice VIII. As the authors indicate, this is a feature that is not yet observed in spectroscopic studies.

The following assessment of the field by Nelmes et al.[3] from 10 years ago remains largely true today: "...although site disordering of some form appears necessary to account for the reproducibly low value of the apparent O−D distance in ice VII, there is, as yet, no clear direct evidence for it, and the detailed nature of this key structure remains unknown." In an attempt to understand experimental findings and shed light on the nature of the static motion of the oxygen atoms in ice VII, we have developed a model that predicts the oxygen displacement from a perfect lattice site as a function of the surrounding H-bond network. Looking at the distance over which H-bond topology affects the site geometry, we find good agreement between the model and ab initio data including only the effects of nearest-neighbor waters. Despite its simplicity, this scheme gives a model for oxygen site displacements that is richer than either of the simple ⟨100⟩ or ⟨111⟩ models previously used to analyze diffraction data. Earlier, Kuo and Klein reported average bond distances and angles and root-mean-square deviations based on periodic density functional theory (DFT) calculations for unit cells of ice VII consisting of 16 water molecules.[4] They did not construct a model linking the direction and magnitude of site displacements to the local H-bond topology, as we have, and could not extrapolate their site displacements to the bulk limit. Kuo and Klein also calculated sublattice shifts in ice VIII, and our calculations agree with these earlier results. In Section 2, we review periodic DFT calculations of H-bond configurations of a 32-water ice VII cell, used in previous studies.[5,6] We

† Part of the "Russel Pitzer Festschrift".

* Corresponding author. E-mail: singer@chemistry.ohio-state.edu.

10.1021/jp902863k CCC: $40.75
Published on Web 07/13/2009

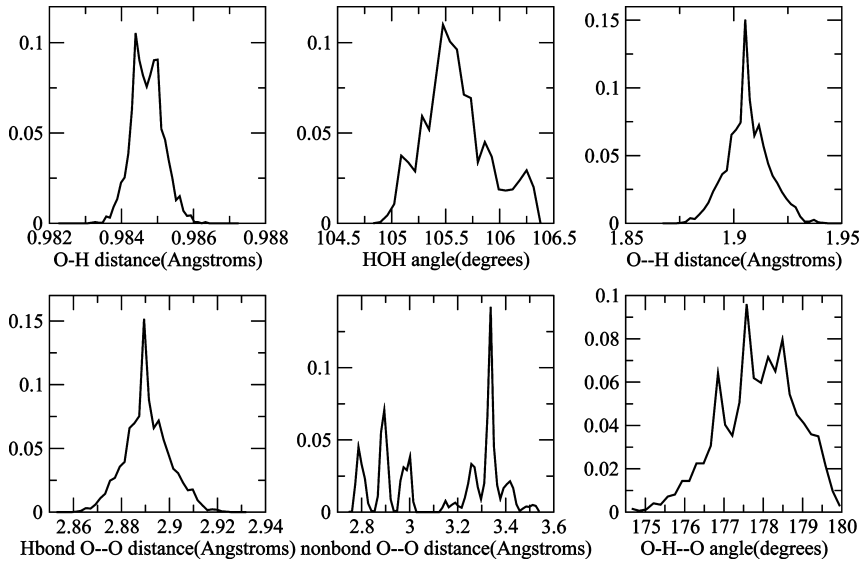

Figure 1. Probability distributions for various geometrical features calculated from the 50 H-bond configurations optimized with a 90 Ry plane wave cutoff.

TABLE 1: Averaged Geometrical Features of H-Bond Configurations of an Ice VII Unit Cell for a Series of Plane Wave Cutoffs[a]

system	covalent O−D (Å)	D−O−D (deg)	H-bonded O−D (Å)	O−D−O (deg)	O−O (Å)
VIII (70 Ry)	0.9889 ± 0.0000	105.92 ± 0.00	1.9016 ± 0.0000	177.30 ± 0.00	2.8898 ± 0.0000
VIII (90 Ry)	0.9844 ± 0.0000	106.24 ± 0.00	1.9061 ± 0.0000	177.56 ± 0.00	2.8898 ± 0.0000
VIII (120 Ry)	0.9837 ± 0.0000	106.25 ± 0.02	1.9068 ± 0.0008	177.56 ± 0.02	2.8898 ± 0.0008
VII (70 Ry)	0.9893 ± 0.0004	105.34 ± 0.30	1.9021 ± 0.0090	177.72 ± 1.03	2.8907 ± 0.0085
VII (90 Ry)	0.9847 ± 0.0004	105.61 ± 0.31	1.9066 ± 0.0098	177.87 ± 0.99	2.8908 ± 0.0093
VII (120 Ry)	0.9840 ± 0.0004	105.59 ± 0.30	1.9073 ± 0.0100	177.88 ± 0.98	2.8908 ± 0.0096

[a] Geometrical properties labeled ice VIII were averaged over the 32-water configuration corresponding to the experimental ice VIII structure with error bars indicating one standard deviation. Those properties labeled ice VII were averaged over all waters in the 50 H-bond configurations studied here. The O−O distances reported are H-bonded oxygen−oxygen distances.

develop and parametrize a model in Section 3 that describes the displacements of oxygen atoms from their perfect lattice sites. In Section 4, we discuss the results of statistical mechanical calculations on a large simulation cell, where we use graph invariants to describe H-bond fluctuations. We conclude with a discussion of the results in Section 5.

2. Periodic Density Functional Theory Calculations

In the hydrogen bond-disordered phase ice VII, there are roughly $(3/2)^N$ hydrogen bonding arrangements possible that satisfy the Bernal−Fowler ice rules[7,8] that each water donates two hydrogen bonds and accepts two hydrogen bonds. This large degeneracy arises because there are six ways to orient a water molecule at each of the lattice sites before the constraints of the ice rules are applied. Theoretical treatment of the H-bond order−disorder transitions among ice phases requires a scheme to calculate the relative energy and structure of the different H-bond arrangements, which we describe in this section, and then a method to handle the statistical mechanics of H-bond fluctuations, which is presented later. We have previously shown that DFT is capable of predicting the ground state and giving a reasonable estimate of the transition temperature for the ice Ih/XI,[5,6] ice VII/VIII,[5,6] ice III/IX,[9] and ice V/XIII[10] phase transitions.

50 H-bond configurations used in a previous study of the ice VII/VIII proton ordering phase transition[5,6] were used to parametrize the oxygen site disorder model developed below. The configurations were selected to cover the full range of energies among the H-bond arrangements in ice VII. We recapitulate some details of the calculations here for convenience. The ice VII unit cell measures $2\sqrt{2} \times 2\sqrt{2} \times 2$ primitive cells on each side consisting of 32 water molecules with lattice constant $a = 3.337$ Å. Periodic DFT calculations were performed on 50 configurations using the CPMD[11−13] program with the Becke−Lee−Yang−Parr gradient correction[14,15] to the local density approximation, Troullier−Martins norm-conserving pseudopotentials,[16] and plane wave cutoffs of up to 120 Ry. The increased cutoff relative to the 70 Ry cutoff used in the previous studies,[5,6] was used to ensure convergence of the geometries. The Brillouin zone sampling was restricted to the Γ point.

From the optimized geometries, probability distributions of certain distances and angles were calculated and are shown in Figure 1. Averages of the distances and angles over the 50 configurations used in periodic DFT calculations are presented in Table 1. (After developing a model linking site displacements to H-bond topology in Section 3, we will provide distributions and averages obtained from a more rigorous theory for thermal distributions in Section 4.) The data in Table 1 show a decreasing change with increasing plane wave cutoff, suggesting that we have nearly reached convergence with respect to geometrical properties. We find that the H-bonded oxygen−oxygen probability distribution has a single peak with an average of 2.8908 ± 0.0093 Å. We do not see evidence of a bimodal distribution of H-bonded distances with a peak separation of ∼0.2 Å, as suggested by Nelmes et al.[3] Kuo and Klein have previously reported a unimodal distribution of H-bond distances in their periodic DFT calculations for ice VII.[4] In contrast with the H-bonded oxygen−oxygen distances, analysis of the non-

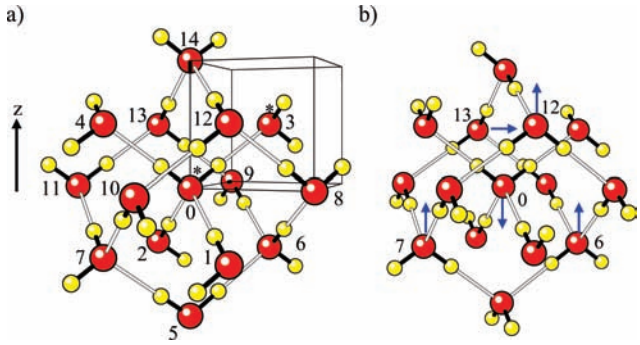

Figure 2. (a) Nearest H-bonded neighbors (1−4) and nearest non-H-bonded neighbors (5−14) surrounding a central water labeled "0". We refer to the orientation of the central water, dipole pointing in the $+z$ direction and hydrogen bonds along the ⟨111⟩ axes, as the "canonical" orientation. Water molecules labeled with asterisks are those that make up the primitive unit cell of ice VII, which the thin black lines outline. (b) Arrows on the central water and its four nearest nonbonded neighbors indicating the direction of the site displacements, as discussed in the text. The water labeled "13" has its dipole vector in the *xy* plane, whereas the other labeled waters (0, 6, 7, 12) have their dipoles pointing along the z axis.

bonded oxygen−oxygen distances shows three peaks, each separated by ∼0.1 Å with the central peak located very close to the H-bonded oxygen−oxygen distance. Average oxygen−oxygen distances for the nearest nonbonded peaks, shown in Figure 1, are 2.7956 ± 0.0153, 2.8928 ± 0.0126, and 2.9855 ± 0.0154 Å. As discussed below, the largest component of the oxygen site displacement is in a direction opposite to the water dipole vector. When nearest-neighbor nonbonded waters have dipoles pointing toward each other, similar to waters labeled "0" and "12" in Figure 2b, the oxygen atoms are displaced away from each other, giving rise to the peak near 2.99 Å. When the dipoles point away from each other, like waters labeled "0" and "6" (also "0" and "7") in Figure 2b, the displacements push the waters closer, generating the peak near 2.79 Å. Dipoles oriented in the same direction result in a nonbonded oxygen−oxygen distance almost unchanged from the hydrogen-bonded distance. Orientations of dipoles whose dot product is zero, like waters "0" and "13", can have distances of 2.89 Å or either 2.79 or 2.99 Å if the dipole of one of the waters points away from or toward the nonbonded neighbor, respectively. The O−O distances when dipoles are perpendicular overlap the previous cases. The three peaks in the nearest-neighbor nonbonded oxygen−oxygen distance distribution were not mentioned in the work of Kuo and Klein.[4]

The next set of peaks among the nonbonded O−O distances in Figure 1 (and more clearly, the thermally averaged distributions below in Figure 4b) break into a quintet ranging from 3.17 to 3.51 Å. This group of nonbonded O−O distances arises from next-nearest nonbonded waters. In Figure 2a, waters 5, 8−11, and 14 are next-nearest nonbonded neighbors of central water 0. Because the dipole moment of water 0 points upward and hence the molecule is displaced downward toward water 5 in Figure 2, distances to water 5 contribute to the smallest three members of the quintet, depending on whether the dipole moment of water 5 points toward or away from water 0. Similarly, because water 0 is displaced away from water 14, distances to water 14 contribute to the largest three members of the next-nearest nonbonded O−O distance quintet. The central water is very weakly displaced in the horizontal plane in Figure 2, and hence waters 8−11 all contribute to the central three peaks of the quintet.

3. H-Bond Model for Site Displacements

To model the oxygen site displacement, we seek an expression that accounts for the surrounding H-bond network of a given water molecule. In previous work,[5,6,9,17−21] we have shown that an economical description of the dependence of scalars, like the energy, on hydrogen bond topology can be developed. The key for describing scalars such as the energy is to form combinations of variables that capture the orientation of H-bonds that are invariant to all symmetry operations of the appropriate space group. We refer to these combinations as graph invariants.[17] Here we extend that idea by forming combinations of H-bond variables that transform as a first-rank tensor. The simplest function that captures how the displacement vector, $\mathbf{d}_0$, depends on the local H-bond topology is a linear combination of H-bond vectors. Higher-order combinations that transform as a first-rank tensor can be generated with group theoretical projection operators,[17,18] but we have found that the lowest-order linear description given in the following equation is adequate to describe site disorder in ice VII.

$$\mathbf{d}_0 = \mathbf{c}_0\hat{\mu}_0 + \sum_{i=1}^{2}\mathbf{c}_i\hat{\mu}_i + \sum_{i=3}^{4}\mathbf{c}_i\hat{\mu}_i + \sum_{i=5}^{14}\mathbf{c}_i\hat{\mu}_i + \ldots \quad (1)$$

The $\mathbf{c}_i$ values are 3 × 3 coefficient matrices, and $\hat{\mu}_\mathbf{i}$ is a unit vector in the direction of the dipole of the ith water. The indices are defined in Figure 2. The dipole vectors are used to describe the local H-bond topology, and an electrostatic model is not implied here. The leading term in the expression is a multiple of the dipole vector of the water whose site displacement is being described. It is found that the water is displaced in a direction opposite to the direction of the dipole, bringing the center of mass of the molecule closer to the perfect lattice site. Keeping only this leading term in the expression results in a model that is identical to the ⟨100⟩ model used to fit experimental data.

$$\mathbf{d}_0^{\langle 100\rangle} = \mathbf{c}_0\hat{\mu}_0 \quad (2)$$

The next two terms in eq 1 arise from nearest neighbors on the same sublattice that donate and accept hydrogen bonds, respectively. Each of these four waters can take only three of the six allowed orientations because of the ice rules, resulting in 81 possible displacements from the set of ⟨100⟩ axes. The next term in the expression comes from the 10 closest neighbors found on the other sublattice, which were divided into 5 groups of waters depending on their height with respect to the z axis. We found no significant improvement in fitting the oxygen site displacement when additional waters were included in the linear model.

We determined the coefficient matrices, the **c** values in eq 1, by minimizing the least-squares error defined in the following expression

$$\text{error} = \sum_{i}^{\text{config}}\sum_{j}^{\text{water}}\{[\mathbf{R}_j + \mathbf{d}_j^{(i)}] - [\mathbf{r}_j^{(i)} + \mathbf{s}^{(i)}]\}^2 \quad (3)$$

where the index i runs over the 50 H-bond configurations and j over the 32 water molecules per configuration. The perfect lattice positions, $\mathbf{R}_j$, for the jth water were generated using the lattice constant a = 3.337 Å, the same lattice constant as that

TABLE 2: Matrix Elements for the Coefficient Matrices, the c Values in Equation 1, for the Oxygen Displacement, in Units of Angstroms, for a Water Molecule in the Canonical Orientation, as Shown in Figure 2[a]

waters	c_{11}	c_{12}	c_{33}
0	0	0	−0.066448
1−2	−0.002364	−0.001471	−0.002988
3−4	−0.002958	−0.001638	−0.002810
5	−0.014633	−0.011808	−0.005692
6−7	0.009234	0.002886	0.004153
8−11	0.000877	0.004144	0.001070
12−13	−0.002114	−0.001427	0.004555
14	0.011005	−0.006850	0.004024

[a] These coefficients were obtained using the geometries calculated with a 90 Ry plane wave cutoff.

used in the periodic DFT calculations. The displacement of the oxygen from its perfect lattice site, $\mathbf{d}_j^{(i)}$, for the jth water in the ith configuration was defined in eq 1. $\mathbf{r}_j^{(i)}$ is the position of the jth water in the ith configuration in the optimized geometry obtained from periodic DFT calculations. A translation for each H-bond configuration, $\mathbf{s}^{(i)}$, was included to account for any overall translation of the system that may have occurred during the geometry optimization. All coefficient matrices could be taken to be of the form

$$\mathbf{c} = \begin{pmatrix} c_{11} & c_{12} & 0 \\ c_{12} & c_{11} & 0 \\ 0 & 0 & c_{33} \end{pmatrix}$$

without any degradation in quality of fit to the data. This property is expected on symmetry grounds because reflections or rotations of the components of water dipole describing the local H-bond topology that lie in the xy plane should not affect the displacement of the central water in Figure 2 along the z direction. Because we divide the 15 waters shown in Figure 2 into 8 unique contributions, this leads to a total of 22 independent parameters, which are listed in Table 2. The coefficient matrix for the water labeled "0" has only one nonzero entry, c_{33}, because $\hat{\mu}_0$ is taken to be parallel to the z axis in the canonical orientation. If this was the only term used in the model, then this nonzero entry would correspond to the site displacement magnitude, $|\mathbf{d}_0^{\langle 100\rangle}|$, in the $\langle 100\rangle$ model discussed above. Fitting the data to the $\mathbf{d}_0^{\langle 100\rangle}$ model gave $c_{33} = -0.076$ Å, which is only slightly larger than the corresponding coefficient in Table 2.

There are two ways to measure the degree to which our model links site displacements to H-bond topology: (1) prediction of the displacements in their original crystal lattice orientation from perfect lattice positions and (2) rotation of each water into the canonical orientation defined in Figure 2a and then measuring the displacement from the perfect lattice position. In the former case, the displacements range from −0.1 to +0.1 Å. The displacements of waters in their original crystal lattice orientation take place with equal magnitude in six directions from the perfect lattice sites. In the latter case, because the waters are now oriented in the same way and the displacement largely occurs in a direction opposite to the water dipole, the displacements now range from −0.1 to 0 Å in the z direction, the direction of the dipole in the canonical orientation, and are much smaller in the x and y directions. The ability of the site displacement model to fit displacements from periodic DFT calculations is demonstrated in Figure 3 for water molecules in their original crystal lattice orientation (top three panels) and the canonical orientation (bottom three panels). The largest disagreement between the model displacements and the optimized structures is 0.03 Å, with only 3% of oxygens having deviations larger than 0.02 Å. The bottom three panels of Figure 3 compare oxygen displacements after the coordinate system is rotated to the same orientation with respect to the perfect lattice orientation. The deviations now lie within a narrow range and are plotted on a magnified scale in the panels, so the scatter of data points appears to be magnified as well. The root-mean-square (rms) deviation of our site displacement model from ab initio data was 3.75×10^{-3} Å. When a simple $\langle 100\rangle$ model was used to fit the ab initio structures, the rms deviation increased three-fold to 1.17×10^{-2} Å. The largest disagreement obtained using predictions from the simple $\mathbf{d}_0^{\langle 100\rangle}$ model was 0.04 Å, with 38 and 5% of oxygens having deviations larger than 0.02 and 0.03 Å, respectively.

4. Statistical Mechanical Results

A previously developed theory for predicting the energetics of H-bond arrangements in ice VII and VIII[5,6] allows us to generate Boltzmann-weighted distributions of H-bond arrangements in ice VII. Using the site displacement model of the previous section, we can now generate thermally averaged site dispacements. We performed Metropolis Monte Carlo simulations on a simulation cell measuring 8 primitive cells on each side containing 1024 water molecules. Results reported below were obtained from simulations at 300 K. Data obtained at 300 K for ice VII showed only minor effects of partial H-bond ordering, in line with the fact that only 7% of the configurational entropy is lost before the ice VIII ordering transition in our simulations.[5,6] Additional simulation details, including a description of the graph invariant expression used here to describe H-bond fluctuations, are identical to those found in previous works on the ice VII/VIII proton ordering transition.[5,6] Using the site displacement model developed here, we calculated equilibrium distributions for the site displacement and oxygen−oxygen distances. As seen in Figure 4, the probability distributions obtained from the statistical mechanical simulations are very similar to those obtained from ab initio calculations on 50 H-bond configurations chosen "semi-randomly" for the 32-water cell. For the oxygen site displacement distribution, the peak near 0.1 Å in the data for the optimized geometries is mostly due to ice-VIII-like H-bond configurations, those with most neighboring water dipoles pointing in the same direction, which are rarely sampled at temperatures above the ordering transition. The 3D probability distribution of the atomic center of oxygen displaced from its perfect lattice site, obtained from Monte Carlo simulations at 300 K, is shown in Figure 5a. The probability distribution is spread across six sites, which are located on the $\langle 100\rangle$ axes as discussed above. As one looks down an axis, the z axis for example, one can see a four-fold symmetry in the probability density. Contour plots, projection onto the xy plane, of the lobes lying on the negative x axis and positive z axis are shown in Figure 5b,c. In both contours, the largest probability of finding the oxygen center is found to lie on the axes with probability decreasing away from the axis. The four-fold symmetry is clearly seen in the contour plot of the lobe located on the positive z axis viewed down the z axis.

5. Discussion

This work has described how the displacement of an oxygen atom from its perfect lattice site, as obtained from periodic DFT calculations, can be linked to the surrounding H-bond topology.

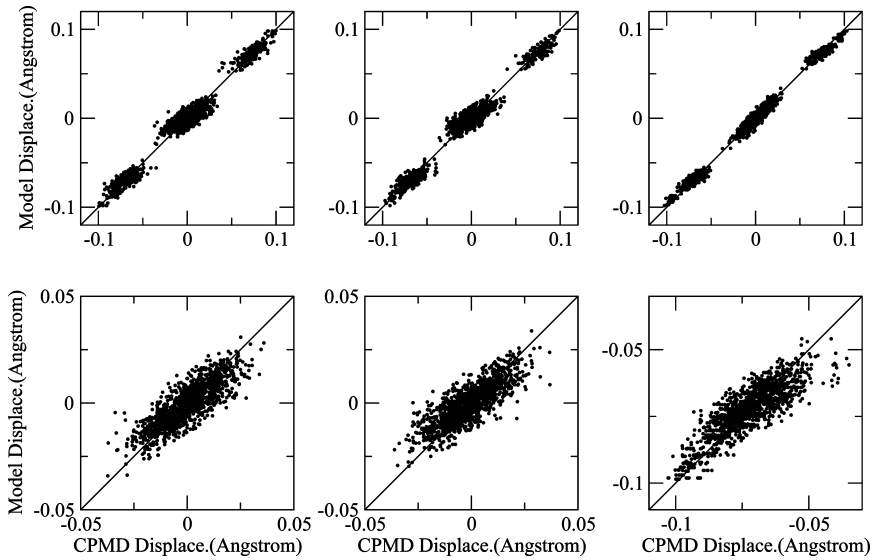

Figure 3. Fit of the oxygen-displacement model to the oxygen displacements of waters in the 50 optimized H-bond configurations. The top row shows the data for waters in their original orientation in the crystal lattice, where the dipoles can point in any one of six directions. The bottom row shows data for all waters in the canonical orientation, where their dipole now points toward positive z. The columns, left to right, show the agreement along the x, y, and z axes, respectively. All points would lie on the straight line if there was perfect agreement.

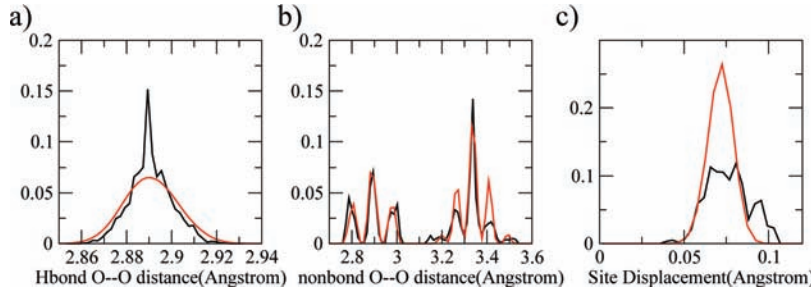

Figure 4. Red curves are the probability distributions for the (a) bonded and (b) nonbonded oxygen−oxygen distances calculated from Monte Carlo simulations at 300 K. The black curves are the same as those shown in Figure 1 to compare with the simulated structure. (c) Probability distribution of the site displacement calculated from 50 H-bond configurations (black) and Monte Carlo simulations (red).

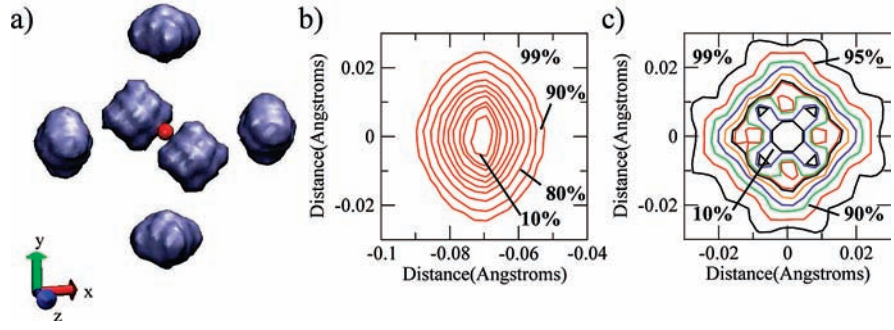

Figure 5. (a) 3D probability distribution of the position of the oxygen centers relative to the perfect lattice site, small red sphere, obtained from Monte Carlo simulations at 300 K. The center of each lobe is located on one of the ⟨100⟩ axes. (b,c) Contour plots of the probability distribution, projected onto the xy plane, of the position of the oxygen centers relative to the perfect lattice site. (b) The oxygen sites closest to the negative x axis, [$\bar{1}$00], with some contours labeled indicating the fraction of oxygen atoms enclosed. The most probable location of the oxygen center is within the contour labeled 10%. (c) The oxygen sites closest to the positive z axis, [001]. In both plots, starting from the contour labeled 90%, the contours decrease in increments of 10% as one looks toward the center of each distribution. For clarity, the 20% contour, nearly identical to the 30% contour, was omitted in part c.

Combined with an analytic technique to describe H-bond fluctuations, graph invariants, we were able to perform statistical mechanical calculations on the site displacement in a large simulation cell. By optimizing the H-bond configurations at increasing plane wave cutoffs, we found that the geometrical features, such as H-bonded oxygen−oxygen distances, are nearly converged by 90 Ry, although other properties, such as the energy and forces, need much larger cutoffs.[22] We find that the oxygen atoms are displaced along the ⟨100⟩ axes and not the recently suggested ⟨111⟩ axes.[3] The maximum of the probability distribution for the site displacement is near 0.071 Å. The hydrogen bonded oxygen−hydrogen and oxygen−oxygen distances have unimodal probability distributions with average lengths of 1.9073 and 2.8908 Å, respectively. The nonbonded oxygen−oxygen probability distribution has three peaks separated by ∼0.1 Å, with the central peak centered at the H-bonded oxygen−oxygen distance. Both of the recently suggested ⟨100⟩ and ⟨111⟩ models are too simplistic. As shown in Figure 5, the

oxygen site distribution has a complex shape. The simple ⟨100⟩ model would replace the complex distribution of Figure 5a with six δ-function peaks. Any model that confines the oxygens to a small number of points along a few lattice directions will not achieve quantitative agreement with diffraction data and will confuse static displacements arising from local variations in H-bond topology with thermal vibrational motion.

Our site displacement model naturally reverts to the geometry of antiferroelectric ice VIII, including the relative displacement of the two sublattices, when the H-bonds are placed in the ice VIII arrangement. With a plane wave cutoff of 90 Ry, our site displacement model predicts a sublattice shift of 0.196 Å, which is in close agreement with a shift 0.205 Å in the original periodic DFT calculations and previous experimental and calculated shifts.[4,23,24] A model parametrized from geometries optimized at a plane wave cutoff of 120 Ry predicts a sublattice shift of 0.203 Å, which improves agreement with the calculated value of 0.204 Å. Therefore, a unified model describes site displacements in both ice VII and ice VIII. We hope that this work will stimulate detailed comparison with neutron diffraction data.

Acknowledgment. We gratefully acknowledge National Science Foundation CHE-0616872 for support of this work and the Ohio Supercomputer Center for resources needed to perform the calculations reported here.

References and Notes

(1) Kuhs, W. F.; Finney, J. L.; Vettier, C.; Bliss, D. V. *J. Chem. Phys.* **1984**, *81*, 3612.

(2) Jorgensen, J. D.; Worlton, T. G. *J. Chem. Phys.* **1985**, *83*, 329–333.

(3) Nelmes, R. J.; Loveday, J. S.; Marshall, W. G.; Hamel, G.; Besson, J. M.; Klotz, S. *Phys. Rev. Lett.* **1998**, *81*, 2719.

(4) Kuo, J.-L.; Klein, M. L. *J. Phys. Chem.* **2004**, *B108*, 19634.

(5) Singer, S. J.; Kuo, J.-L.; Hirsch, T. K.; Knight, C.; Ojamäe, L.; Klein, M. L. *Phys. Rev. Lett.* **2005**, *94*, 135701.

(6) Knight, C.; Singer, S. J.; Kuo, J.-L.; Hirsch, T. K.; Ojamäe, L. P.; Klein, M. L. *Phys. Rev.* **2006**, *E73*, 056113.

(7) Pauling, L. *J. Am. Chem. Soc.* **1935**, *57*, 2680.

(8) Bernal, J. D.; Fowler, R. H. *J. Chem. Phys.* **1933**, *1*, 515.

(9) Knight, C.; Singer, S. J. *J. Chem. Phys.* **2006**, *125*, 64506.

(10) Knight, C.; Singer, S. J. *J. Chem. Phys.* **2008**, *129*, 164513.

(11) Car, R.; Parrinello, M. *Phys. Rev. Lett.* **1985**, *55*, 2471.

(12) Car, R.; Parrinello, M. In *Simple Molecular Systems at Very High Density*; Polian, A., Loubeyre, P., Boccara, N., Eds.; NATO ASI Series B; Plenum: New York, 1989; Vol. 186, p 455.

(13) *CPMD*, Copyright IBM Corp. 1990−2006, Copyright MPI für Festkörperforschung Stuttgart 1997−2001.

(14) Becke, A. D. *Phys. Rev.* **1988**, *A38*, 3098.

(15) Lee, C.; Yang, W.; Parr, R. G. *Phys. Rev.* **1988**, *B37*, 785.

(16) Troullier, N.; Martins, J. L. *Phys. Rev.* **1991**, *B43*, 1993.

(17) Kuo, J.-L.; Coe, J. V.; Singer, S. J.; Band, Y. B.; Ojamäe, L. *J. Chem. Phys.* **2001**, *114*, 2527.

(18) Kuo, J.-L.; Singer, S. J. *Phys. Rev.* **2003**, *E67*, 016114.

(19) Knight, C.; Singer, S. J. *J. Phys. Chem.* **2005**, *B109*, 21040.

(20) Knight, C.; Singer, S. J. In *Physics and Chemistry of Ice*; Kuhs, W. F., Ed.; Symposium on the Physics and Chemistry of Ice; Royal Society of Chemistry: Cambridge, U.K., 2007; p 329.

(21) Knight, C.; Singer, S. J. In *Physics and Chemistry of Ice*; Kuhs, W. F., Ed.; Symposium on the Physics and Chemistry of Ice; Royal Society of Chemistry: Cambridge, U.K., 2007; p 339.

(22) Lee, H.-S.; Tuckerman, M. E. *J. Phys. Chem.* **2006**, *A110*, 5549–5560.

(23) Nelmes, R. J.; Loveday, J. S.; Wilson, R. M.; Besson, J. M.; Pruzan, P.; Klotz, S.; Hamel, G.; Hull, S. *Phys. Rev. Lett.* **1993**, *71*, 1192.

(24) Ojamäe, L.; Hermansson, K.; Dovesi, R.; Roetti, C.; Saunders, V. R. *J. Chem. Phys.* **1994**, *100*, 2128.

JP902863K